



# OPEN Zika virus vertical transmission induces neuroinflammation and synapse impairment in brain cells derived from children born with Congenital Zika Syndrome

Cecilia Benazzato<sup>1</sup>, Fernando Lojudice<sup>2</sup>, Felizia Pöehlchen<sup>1,3</sup>, Paulo Emílio Corrêa Leite<sup>4</sup>, Antonio Carlos Manucci<sup>5</sup>, Vanessa Van der Linden<sup>6</sup>, Patricia Jungmann<sup>7</sup>, Mari C. Sogayar<sup>2,5</sup>, Alexandre Bruni-Cardoso<sup>5</sup>, Fabiele B. Russo<sup>1✉</sup> & Patricia Beltrão-Braga<sup>1,8✉</sup>

Zika virus (ZIKV) infection was first reported in 2015 in Brazil as causing microcephaly and other developmental abnormalities in newborns, leading to the identification of Congenital Zika Syndrome (CZS). Viral infections have been considered an environmental risk factor for neurodevelopmental disorders outcome, such as Autism Spectrum Disorder (ASD). Moreover, not only the infection per se, but maternal immune system activation during pregnancy, has been linked to fetal neurodevelopmental disorders. To understand the impact of ZIKV vertical infection on brain development, we derived induced pluripotent stem cells (iPSC) from Brazilian children born with CZS, some of the patients also being diagnosed with ASD. Comparing iPSC-derived neurons from CZS with a control group, we found lower levels of pre- and postsynaptic proteins and reduced functional synapses by *puncta* co-localization. Furthermore, neurons and astrocytes derived from the CZS group showed decreased glutamate levels. Additionally, the CZS group exhibited elevated levels of cytokine production, one of which being IL-6, already associated with the ASD phenotype. These preliminary findings suggest that ZIKV vertical infection may cause long-lasting disruptions in brain development during fetal stages, even in the absence of the virus after birth. These disruptions could contribute to neurodevelopmental disorders manifestations such as ASD. Our study contributes with novel knowledge of the CZS outcomes and paves the way for clinical validation and the development of potential interventions to mitigate the impact of ZIKV vertical infection on neurodevelopment.

The Congenital Zika Syndrome (CZS) was first described in Brazil in 2015, being considered by WHO as a global health emergency, after thousands of cases of babies born with microcephaly because of their mother's infection during pregnancy with Zika virus (ZIKV)<sup>1</sup>, a member of the Flaviviridae viral family, that usually cause mild symptoms in humans, such as low-grade fever, skin rash, joint pain, and conjunctivitis<sup>2</sup>. CZS is mainly characterized by neurological abnormalities, including microcephaly, severe cortical malformations, ventriculomegaly, cerebellar hypoplasia, and abnormal white matter hypodensity<sup>1,3–5</sup>. In addition, ZIKV infection during pregnancy has been associated with neurodevelopmental disorders outcome<sup>6</sup>, such as Autism Spectrum Disorder (ASD).

ASD is a neurodevelopmental condition characterized by difficulties in social interaction and communication and the presence of restricted interests and repetitive behaviors<sup>7</sup>, typically emerging in early childhood and being

<sup>1</sup>Microbiology Department, Institute of Biomedical Sciences (ICB-II), University of São Paulo, Av. Prof. Lineu Prestes, 1374, 2Nd Floor, Room 235, São Paulo, SP 05508-000, Brazil. <sup>2</sup>Cell and Molecular Therapy Center (NUCEL), School of Medicine, University of São Paulo, São Paulo-SP 01246-903, Brazil. <sup>3</sup>Westfälische Wilhelms-Universität Münster, Münster, Germany. <sup>4</sup>Clinical Research Unit of the Antonio Pedro Hospital, Federal Fluminense University, Rio de Janeiro 24220-900, Brazil. <sup>5</sup>Biochemistry Department, Chemistry Institute, University of São Paulo, São Paulo, SP 05508-900, Brazil. <sup>6</sup>Barão de Lucena Hospital, Recife 50731-900, Brazil. <sup>7</sup>Pathology Department, University of Pernambuco, Recife 50670-901, Brazil. <sup>8</sup>Institute Pasteur of São Paulo, Av. Prof. Lucio Martins Rodrigues 370, A-Building, 4Th Floor, São Paulo-SP 05508-020, Brazil. ✉email: fabielerusso@gmail.com; patriciacbbbraga@usp.br

influenced by genetic and environmental factors. The triggers for ASD outcomes have been investigated, with neuroinflammation being considered as a strong element. One specific cytokine, namely, the proinflammatory Interleukin-6 (IL-6), has been found to be elevated in patients plasma<sup>8</sup>, post-mortem brain<sup>9,10</sup>, cerebrospinal fluid<sup>11</sup>, and in iPSC-derived astrocytes<sup>12</sup> of children diagnosed with ASD. Another cytokine, namely, tumor necrosis factor-alpha (TNF-α), has also been implicated in this condition, since it plays a role in neuronal differentiation and apoptosis, potentially leading to impaired brain function during fetal development<sup>2</sup>. ZIKV infection also induces high levels of proinflammatory immune mediators, such as IL-6, TNF-α, interleukin 1β (IL-1β) and monocyte chemotactic protein 1 (MCP-1) in human fetal brain<sup>3</sup>. Studies have indicated a significant association between intrauterine viral infections and an increased risk of ASD<sup>7</sup>.

In the present work, we aimed at investigating the CNS of children born with CZS in order to shed light on the pathogenicity of ZIKV and its impact on neurodevelopment. We hypothesized that ZIKV infection during fetal neurogenesis may lead to significant alterations in CNS cells, probably causing permanent damage to their function, eventually being compatible with the ASD phenotypes. This damage may arise from the infection itself or because of the immune response of the mother<sup>4</sup>, which possibly causes epigenetic changes. To explore the correlation between CZS and ASD, we took advantage of the induced pluripotent stem cells (iPSC) technology.

To that end, we isolated fibroblasts from infants born with the CZS, previously diagnosed (or not) with ASD. Subsequently, we reprogrammed the fibroblasts into iPSC and differentiated them into brain cells, such as neural progenitor cells (NPC), neurons, and astrocytes, to investigate their cell functioning profile.

**Results**  
**NPC derived from CZS patients and controls showed similar expression of molecular and cellular markers**

To be included in the study, the infants should have been born alive with microcephaly resulting from CZS. These patients were chosen based on their clinical features (Table 1). The controls (CTRL) used for this study were previously recruited<sup>8</sup>.

Fibroblasts isolated from CZS patients were reprogrammed into iPSC (Fig. 1A,B), being characterized prior to differentiation. IPSC from CTRL individuals and CZS patients expressed Nanog, Sox2, Lin 28 and Oct4, confirming the cell reprogramming success (Fig. 1C,D). Neural Progenitor Cells (NPC) derived from iPSC from CTRL and CZS were produced using the protocol described elsewhere<sup>12,22</sup>, illustrated in Fig. 1E. NPC revealed expression of Nestin, Sox2, and Musashi 1 (MS-1) and did not express MAP-2, confirming the NPC differentiation success (Fig. 1F,G).

	CZS/A		CZS/B	
	CZS1	CZS2	CZS3	CZS4
General information				
Sex	M	M	M	M
Microcephaly	Yes	Yes	Yes	Yes
Microcephaly diagnosis	Intrauterine—8th gestational month	Intrauterine—8th gestational month	Intrauterine—7th gestational month	At Birth
IgM anti-ZIKV (at birth)	IgG +	IgG +	IgG +	IgG +
Developmental history				
Irritability	Yes	Yes	Yes	Yes
Hyperexcitability	Yes	No	Yes	Yes
Dysphagia	Yes	Yes	Yes	Yes
Eye injury	No	No	No	Yes—Visual impairment
ASD diagnosis	No	No	Yes	Yes
Convulsive crisis	Yes	No	Yes	Yes
Hydrocephalus	No	No	No	Yes
Additional remarks	–	Severe arthrogryposis,—dislocation of hip joints, strabismus	–	Frontal cortex with severe malformation, severe arthrogryposis and bilateral cryptorchidism
Pregnancy history				
Maternal age	26 years old	18 years old	34 years old	18 years old
Length/Weight	48 cm/ 2785 g	44 cm/ 2790 g	48 cm/2745 g	41 cm/2350 g
Maternal fever	Yes, on 2nd month of pregnancy	Yes, on 4th month of pregnancy with rash and diarrhea	Yes, on 4th month of pregnancy	No
Drugs	No	No	No	No
Medicine during pregnancy	No	No	No	No
Family history				
Family member with neurological diseases	No	No	No	No

**Table 1.** Summary of Clinical Features for the Participants.

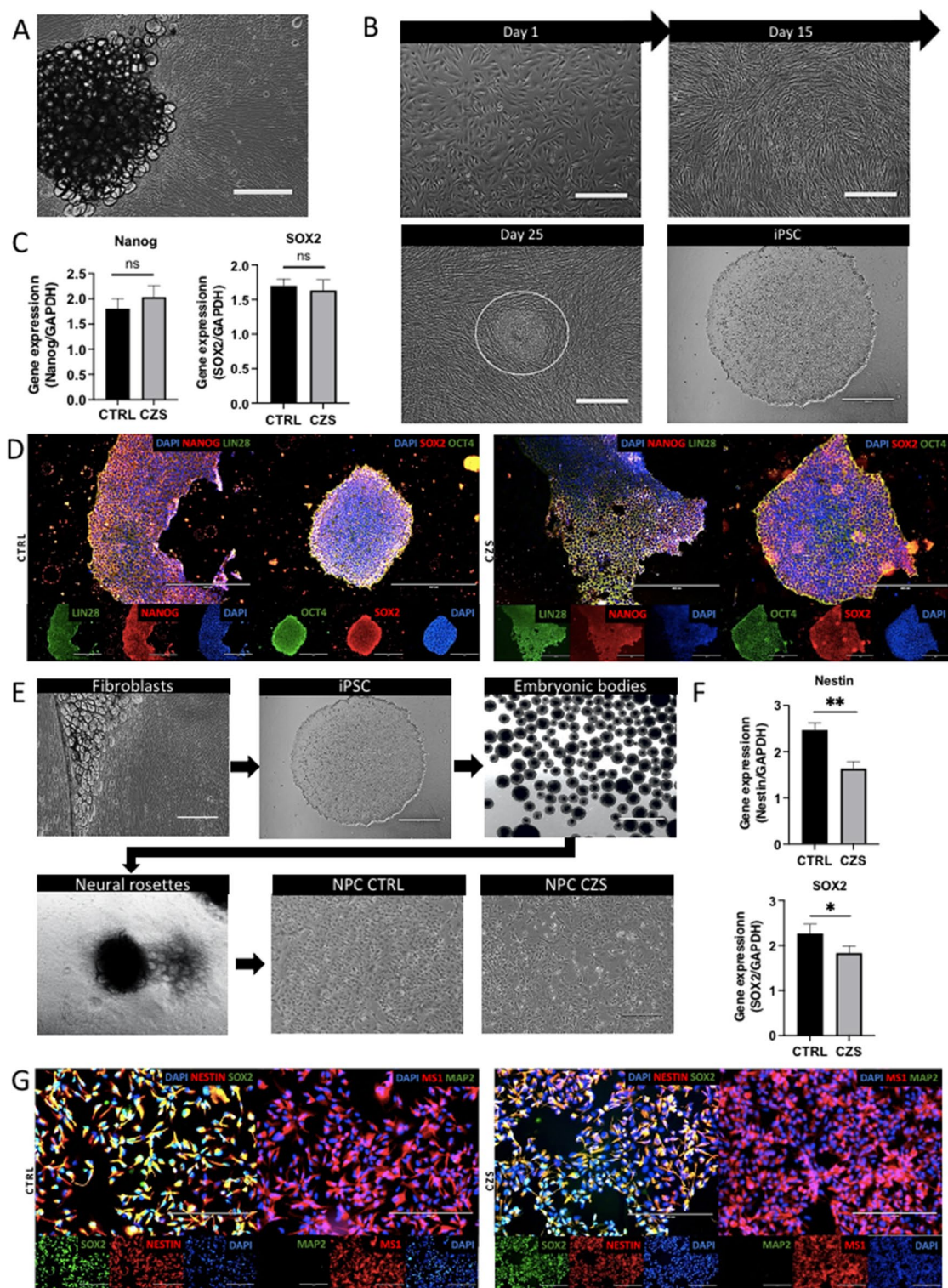


**Figure 1.** Reprogramming of CZS fibroblasts from skin biopsies into iPSC and differentiation into NPC. (A) Representative image of fibroblasts derived from skin explants from patients with CZS. (B) Representative image of the establishment of iPSC colonies from CZS patients. (C) Gene expression of for Nanog and SOX2 in iPSC by qRT-PCR. (D) Representative image of iPSC colonies shown in C, and LIN28, NANOG, OCT4, and SOX2 gene expression for all samples used in this study. (E) Representative images of morphological changes during the NPC production steps. (F) NPC displaying expression of the Nestin and SOX2 NPC markers. (G) Representative image of NPC by immunofluorescence. The NPC obtained displayed SOX2, Nestin, and Musashi 1 expression in all samples used in this study. MAP2, known as a neuron marker, was not expressed in NPC. (A, B, D, E) Objective magnification: 4x. 200  $\mu$ m scale bars. (G) Objective magnification: 20x. 50  $\mu$ m scale bars.



**Figure 2.** CZS-derived neurons display reduced synaptogenesis, less glutamate production and differential astrocyte quantification. (A) Representative images depicting morphological changes during neuronal differentiation. (B) Gene expression upon neuronal differentiation. Cell culture showed expression of MAP2, a neuronal marker and low expression of Musashi1, an NPC marker. (C) Representative image of mixed culture upon neuronal differentiation, characterization by immunofluorescence. Cells revealed expression of MAP2, a neuronal marker, and low staining for GFAP, a glial marker, in both CTRL and CZS/A groups, and even less GFAP in the CZS/B group. None of the groups showed expression for Musashi1, a progenitor cell marker. (D) Correlation between CZS groups and CTRL neuronal cell lines (% of MAP2 and GFAP positive cells). It is possible to observe that the CZS/A group has similar proportions of cells when compared to the CTRL ( $p=0.3131$ ), while the CZS/B group showed a significant reduction of GFAP compared to the CTRL ( $p=0.0065$ ). (E) Synapsin 1 (pre-synaptic) and PSD-95 (postsynaptic) gene expression in neurons upon 4 weeks of differentiation, by qRT-PCR/ $\Delta\Delta C_t$ . A significant reduction in the expression levels of both genes was found in the neurons of patients with CZS (both CZS/A and CZS/B), when compared to the CTRL (Synapsin 1: CZS/A:  $p=0.0363$ ; CZS/B:  $p=0.0264$  / PSD95: CZS/A:  $p=0.0130$ ; CZS/B:  $p=0.0118$ ). (F) Representative image of *puncta* co-localization, showing the expression of MAP2 (white), Synapsin 1 (green) and PSD-95 (red). (G) Analysis of synaptic *puncta* counting. Synapsin1 was reduced in CZS groups (CZS/A  $p<0.0001$ , CZS/B  $p<0.0001$ ). PSD95 was reduced in CZS groups ( $p<0.0001$ ) and even more reduced in CZS/B, when compared to the CZS/A ( $p=0.0488$ ). Both functional *puncta* and co-localization were reduced in both CZS groups, when compared to the CTRL (CZS/A,  $p<0.0001$  / CZS/B,  $p<0.0001$ ). Lastly, CZS/B showed even less functional *puncta* quantification than CZS/A ( $p=0.1750$ ). (H) Analysis of glutamate production in the supernatant of neuronal culture. CZS groups presented a reduction in glutamate production, when compared to the CTRL group (CTRL vs. CZS1- 1 h:  $p=0.0891$ ; 24 h:  $p=0.0522$ ; 48 h:  $p=0.0655$ ; 72 h:  $p=0.0584$ ; 96 h:  $p=0.0530$  / CTRL vs. CZS2- 1 h:  $p=0.1079$ ; 24 h:  $p=0.1120$ ; 48 h:  $p=0.3017$ ; 72 h:  $p=0.1841$ ; 96 h:  $p=0.1645$  / CTRL vs. CZS3- 1 h:  $p=0.0401$ ; 24 h:  $p=0.1211$ ; 48 h:  $p=0.9999$ ; 72 h:  $p=0.7336$ ; 96 h:  $p=0.5877$  / CTRL vs. CZS4- 1 h:  $p=0.0011$ ; 24 h:  $p=0.2016$ ; 48 h:  $p=0.9913$ ; 72 h:  $p>0.9999$ ; 96 h:  $p=0.9956$ ). Glutamate levels were normalized relative to the total number of cells. (A) Objective magnification: 10x. 100  $\mu\text{m}$  scale bars. (C) Objective magnification: 40x. 20  $\mu\text{m}$  magnification bars. (F) Objective magnification: 63x. 10  $\mu\text{m}$  scale bars. The statistical study was analyzed through Two-way ANOVA (D, H) and One-way ANOVA (E, G).

### Neurons derived from CZS patients presented reduced synaptogenesis

Neuronal differentiation ensued from NPC and were maintained for 30 days in cell culture for complete maturation (Fig. 2A). Evaluation of gene expression showed similar levels of MAP2 between CTRL and CZS and low levels of Musashi1, revealing the achievement of cell differentiation (Fig. 2B). The immunofluorescence results were quantified in order to analyze the relative proportion of neurons and astrocytes, since the protocol yields a mixed cell population (Fig. 2C). Usually, the differentiation protocol yields around 80% of neurons and 20% of astrocytes, but total cell counting considering the MAP2 and GFAP ratio was carried out to confirm this (Fig. 2D). Intriguingly, two out of four CZS patients did not exhibit levels of GFAP labeling. Consequently, they were divided into two subgroups: the GFAP-labeled group (CZS/A, comprising CZS1 and CZS2) and the non-GFAP-labeled group (CZS/B, comprising CZS3 and CZS4) for further analysis (Fig. 2D). Interestingly, the CZS/B patients who presented astrogenesis impairment were also the ones diagnosed with ASD, as showed in Table 1.

Synapse quantification assay was conducted to evaluate potentially different phenotypes between the two conditions and neuronal functionality, assessing presynaptic (Synapsin 1) and postsynaptic (PSD-95) gene expression array by qRT-PCR. Our results showed that the CZS groups expressed lower levels of Synapsin 1 and PSD-95 compared to CTRL (Fig. 2E).

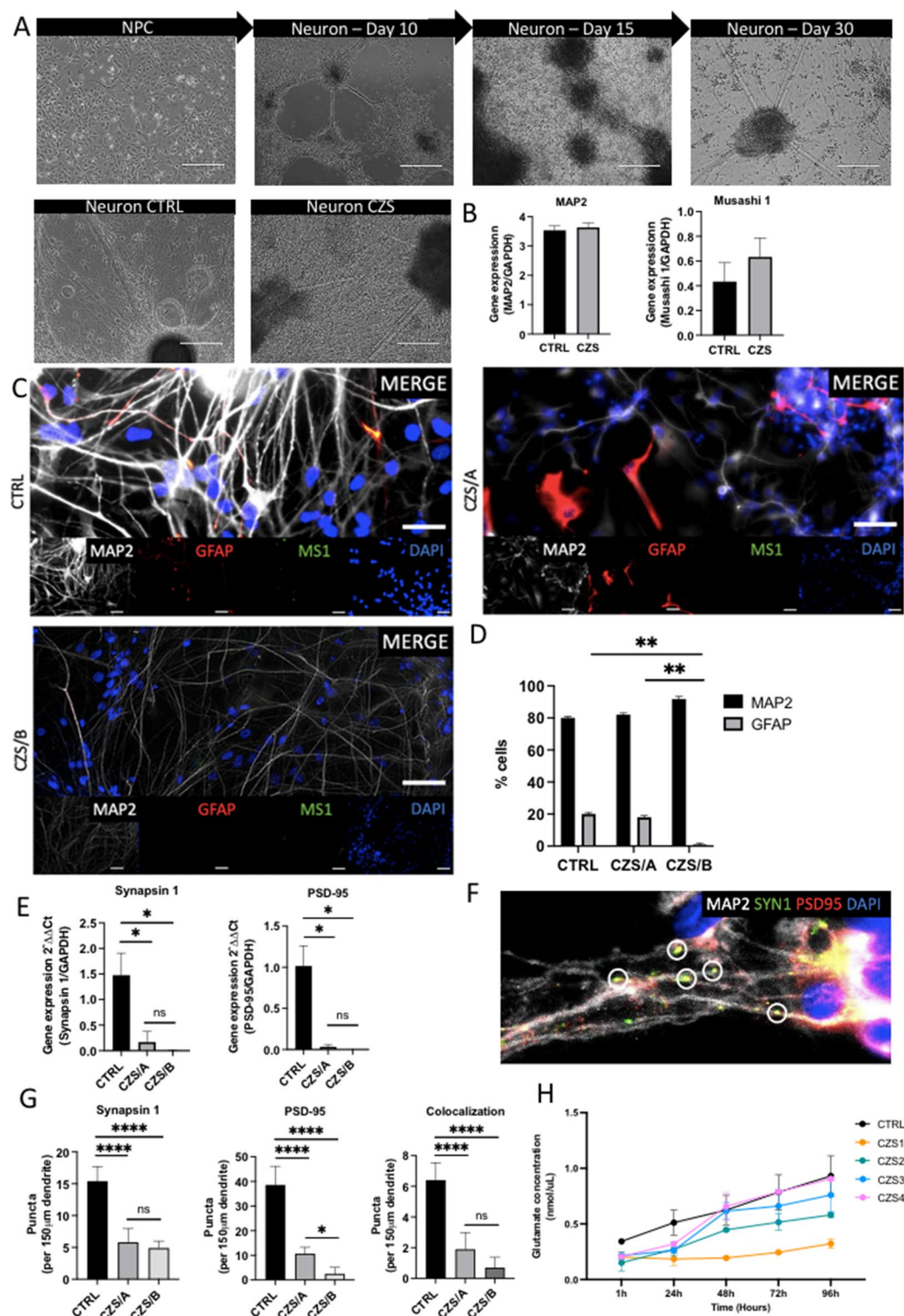
Synaptic events were analyzed by immunostaining of presynaptic protein (SYN1) and postsynaptic protein (PSD-95) on neuronal dendrites, evidenced by MAP2 staining (Fig. 2F). These results indicate a significant reduction in the presynaptic protein Synapsin 1 in the neurons of both CZS/A and CZS/B groups compared to the CTRL. Similarly, we found a significant decrease in the PSD-95 postsynaptic protein in both the CZS/A and CZS/B groups, when compared to the CTRL group, with the CZS/B group showing even a lower expression compared to the CZS/A one. In addition, analysis of pre- and postsynaptic markers showed a pronounced decrease of *puncta* co-localization in the CZS patients compared to the CTRL ones, which probably leads to a connectivity impairment (Fig. 2G).

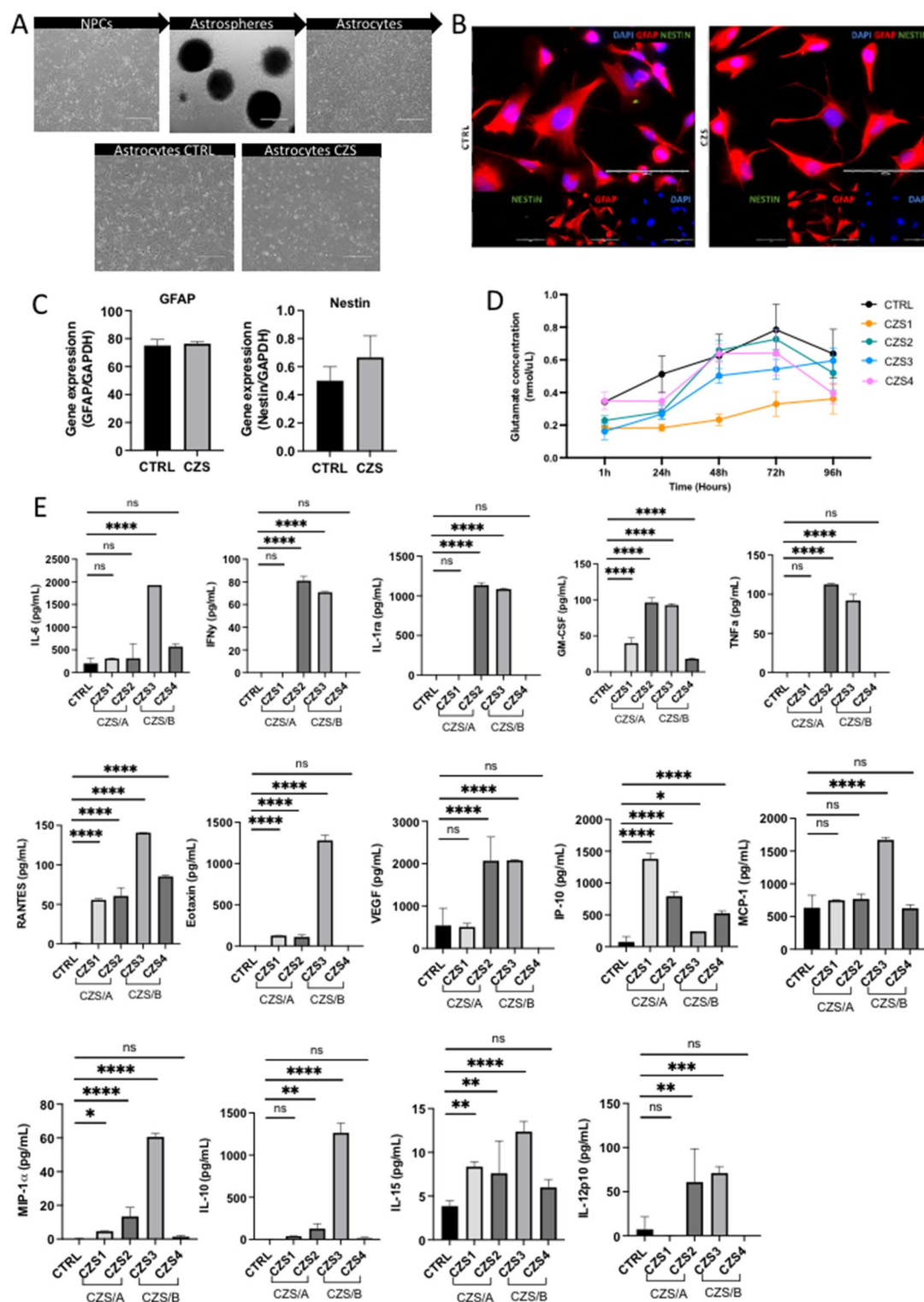
Glutamate, the main excitatory neurotransmitter in the brain, is an additional factor that could lead to further physiological impairments of neuronal cells. Our analyses revealed a tendency of glutamate reduction in the supernatant of CZS-derived neurons, when compared with the CTRL one (Fig. 2H).

### Astrocytes derived from CZS patients presented changes in glutamate and cytokine production

Astrocytes were produced using a specific protocol established by our group<sup>12</sup> as illustrated in Fig. 3A. At the end of the protocol, astrocytes were characterized by immunofluorescence and qRT-PCR, comparing the expression of specific markers for astrocytes and their progenitors, the NPC. The results demonstrated that astrocytes expressed GFAP, a specific glial cell marker, while exhibiting lower expression of Nestin (Fig. 3B,C). Morphologically, astrocytes appeared as stellate and large cells (Fig. 3B).

To evaluate astrocyte physiology, we analyzed the glutamate levels in the supernatant of the cell culture at multiple time points. In cell culture, astrocytes can produce and uptake glutamate<sup>5</sup>. Astrocytes derived from CZS patients showed lower levels of glutamate production in all time points analyzed, compared to the CTRL astrocytes (Fig. 3D).







◀**Figure 3.** CZS-derived Astrocytes display less glutamate and higher cytokine levels. (A) Representative images depicting morphological changes during the astrocyte differentiation protocol. (B) Representative images of astrocytes characterized by immunofluorescence. Astrocytes revealed GFAP expression in CTRL and CZS patients but not of Nestin, an NPC marker. (C) Gene expression upon astrocyte differentiation. Cell cultures displayed expression of GFAP ( $p=0.4541$ ), a glial marker; and low expression of Nestin ( $p=0.3265$ ), an NPC marker. (D) Analysis of glutamate levels in the supernatant of astrocytes culture. Compared to the CTRL, a reduction in glutamate levels was found at all time points investigated (CTRL vs. CZS1- 1 h:  $p=0.0077$ ; 24 h:  $p=0.0739$ ; 48 h:  $p=0.0668$ ; 72 h:  $p=0.0536$ ; 96 h:  $p=0.1580$  / CTRL vs. CZS2- 1 h:  $p=0.0535$ ; 24 h:  $p=0.1220$ ; 48 h:  $p=0.5048$ ; 72 h:  $p=0.2292$ ; 96 h:  $p=0.9711$  / CTRL vs. CZS3- 1 h:  $p=0.0443$ ; 24 h:  $p=0.1301$ ; 48 h:  $p=0.9777$ ; 72 h:  $p=0.9250$ ; 96 h:  $p=0.6692$  / CTRL vs. CZS4- 1 h:  $p=0.9984$ ; 24 h:  $p=0.2498$ ; 48 h:  $p=0.9991$ ; 72 h:  $p=0.6305$ ; 96 h:  $p=0.2060$ ). Glutamate levels were normalized relative to the total number of cells. (E) Quantification of cytokines in the supernatants of astrocytes. Compared to the CTRL, significantly higher levels of cytokines were found in CZS patients (IL-6—CZS1:  $p=0.8759$ ; CZS2:  $p=0.8596$ ; CZS3:  $p<0.0001$ ; CZS4:  $p=0.0522$ ) (IFN $\gamma$ —CZS1:  $p>0.9999$ ; CZS2:  $p<0.0001$ ; CZS3:  $p<0.0001$ ; CZS4:  $p>0.9999$ ) (IL-1 $\alpha$ —CZS1:  $p>0.9999$ ; CZS2:  $p<0.0001$ ; CZS3:  $p<0.0001$ ; CZS4:  $p>0.9999$ ) (GM-CSF—CZS1:  $p<0.0001$ ; CZS2:  $p<0.0001$ ; CZS3:  $p<0.0001$ ; CZS4:  $p<0.0001$ ) (TNF $\alpha$ —CZS1:  $p<0.0001$ ; CZS2:  $p<0.0001$ ; CZS3:  $p<0.0001$ ; CZS4:  $p<0.0001$ ) (RANTES—CZS1:  $p<0.0001$ ; CZS2:  $p<0.0001$ ; CZS3:  $p<0.0001$ ; CZS4:  $p<0.0001$ ) (Eotaxin—CZS1:  $p<0.0001$ ; CZS2:  $p<0.0001$ ; CZS3:  $p<0.0001$ ; CZS4:  $p>0.9999$ ) (VEGF—CZS1:  $p=0.9998$ ; CZS2:  $p=0.0007$ ; CZS3:  $p=0.0001$ ; CZS4:  $p=0.1228$ ) (IP-10—CZS1:  $p<0.0001$ ; CZS2:  $p<0.0001$ ; CZS3:  $p=0.0125$ ; CZS4:  $p<0.0001$ ) (MCP-1—CZS1:  $p=0.5950$ ; CZS2:  $p=0.4712$ ; CZS3:  $p<0.0001$ ; CZS4:  $p=0.9999$ ) (MIP-1 $\alpha$ —CZS1:  $p=0.0273$ ; CZS2:  $p<0.0001$ ; CZS3:  $p<0.0001$ ; CZS4:  $p=0.8552$ ) (IL-10—CZS1:  $p=0.6818$ ; CZS2:  $p=0.0051$ ; CZS3:  $p<0.0001$ ; CZS4:  $p=0.9851$ ) (IL-15—CZS1:  $p=0.0021$ ; CZS2:  $p=0.0091$ ; CZS3:  $p<0.0001$ ; CZS4:  $p=0.1851$ ) (IL-12p70—CZS1:  $p=0.9474$ ; CZS2:  $p=0.0013$ ; CZS3:  $p=0.0002$ ; CZS4:  $p=0.9406$ ). (B) Objective magnification: 40x. 20  $\mu$ m scale bars. The data were analyzed by Two-way ANOVA (D) and One-way ANOVA (E).

Lastly, we evaluated the astrocyte cytokine profile, since neuroinflammatory cytokines could impact cell functionality and impair brain homeostasis. In general, cytokines released by CZS-derived astrocytes produced a more inflammatory profile than those produced by CTRL-derived cells. Patient CZS1 displayed significant differences in the level of cytokines IFN- $\gamma$ , IL-1 $\alpha$ , GM-CSF, RANTES, eotaxin, IP-10/CXCL10, MIP-1 $\alpha$ , and IL-15, compared to the CTRL group. Patient CZS2 exhibited significant differences in the level of cytokines IFN- $\gamma$ , IL-1 $\alpha$ , GM-CSF, TNF- $\alpha$ , RANTES/CCL5, eotaxin, VEGF, IP-10/CXCL10, MIP-1 $\alpha$ , IL-10, IL-15, and IL-12(p70), compared to the CTRL group. Patient CZS3 exhibited significant differences in the level of IL-6, IFN- $\gamma$ , IL-1 $\alpha$ , GM-CSF, TNF- $\alpha$ , RANTES/CCL5, eotaxin, VEGF, IP-10/CXCL10, MCP-1, MIP-1 $\alpha$ , IL-10, IL-15, and IL-12(p70), compared to the CTRL group. Patient CZS4 demonstrated significant level changes of GM-CSF, RANTES/CCL5 and IP-10/CXCL10 compared to the CTRL group (Fig. 3E).

## Discussion

The connection between ZIKV infection and microcephaly was first reported in Brazil, but even after eight years, a broad knowledge about the neurodevelopment of these individuals in terms of CNS functioning is still lacking. We aimed to explore these gaps by modeling brain cell behavior using the iPSC technology. Currently, iPSC have been used as a tool in different approaches, such as: disease modeling<sup>13</sup>, drug discovery<sup>14</sup> and regenerative cell therapy<sup>15</sup>. iPSC constitutes an excellent tool for studies related to neurodevelopmental disorders, rare diseases, and diseases related to epigenetics and mutations, since this technology can retain the donor cells' genetic background, gene expression and even genetic changes caused by epigenetic effects accounted for in a cell, under cell reprogramming<sup>16,17</sup>. Our approach sought to understand the effects of ZIKV infection during neurodevelopment, while preserving the genetic background of affected patients, which could contribute to an individual's outcome<sup>18,19</sup>.

In this work, iPSC were successfully derived from CZS patients. Upon differentiation of these iPSC, NPC, neurons and astrocytes were derived in order to produce an in vitro model to investigate the mechanism involved in brain functioning of CZS children. To our knowledge, this is the first report using this approach to model CZS patients to investigate their neurodevelopment. It is important to mention that we did not use ZIKV to infect CNS-derived cells, as previously reported<sup>20–22</sup>. In our study, gene expression of Nanog and SOX2, by qRT-PCR, and LIN28, NANOG, OCT4, and SOX2, by immunofluorescence assay were performed for iPSC characterization. Gene expression for Nestin and SOX2, by qRT-PCR, and SOX2, Nestin, Musashi 1, and MAP2, by immunofluorescence assay were assessed for NPC characterization.

In order to evaluate the neuronal behavior, NPC were submitted to neuronal differentiation protocol, which produces a mixed cell population composed of around 80% of neurons and 20% of astrocytes, the latter being essential for neuronal functioning<sup>12,23</sup>. We first explored this balance between the two conditions, namely: CZS and CTRL. The neuronal differentiation revealed an equivalent number of neurons between the two conditions. Interestingly, we observed different numbers of astrocyte production among the four CZS patients, verified by evaluating the astrocyte-specific marker GFAP. This led us to divide the CZS patients into two new groups, CZS-A and CZS-B (with reduced astrocytes staining in the cell culture).

The presence or absence of astrocytes in neuron cultures can influence neuronal function<sup>12</sup>, and thus synaptogenesis. Therefore, we further investigated the chemical synapses by qRT-PCR and immunofluorescence to assess the expression of pre- and postsynaptic genes (Synapsin 1 and PSD-95). The qRT-PCR results revealed a significant decrease in the expression of these genes in CZS patients, when compared to the control group,

indicating a potential reduction in synapse formation in these patients. This finding aligns with previous *in vitro* studies on neurons and astrocytes derived from patients with neurodevelopmental disorders, such as ASD<sup>12,24</sup> and Rett syndrome<sup>23</sup>. Furthermore, immunofluorescence allowed us to quantify synaptic events by manually counting the number of pre- and postsynaptic proteins and their co-localization, representing the functional synapses.

The results demonstrated a significant decrease in the number of presynaptic and postsynaptic proteins and their co-localization in all CZS patients, when compared to the control group, which revealed an impairment in the synaptogenesis processes for CZS patients. This decrease in synaptogenesis is consistent with previous studies conducted in iPSC-derived cells and mice infected with ZIKV<sup>25,26</sup>. These findings provide insights into the clinical phenotypes observed in CZS patients, such as cognitive deficits, which may result from impaired communication within neuronal networks. Notably, the CZS/A group, which had a similar proportion of neurons and astrocytes within the control group, exhibited more co-localization points and postsynaptic proteins than the CZS/B group, which experienced a significant reduction in astrocyte proportion in the mixed cell culture. Notably, CZS/B patients received an ASD diagnosis (Table 1). Decreased synapses and deficits in the neuronal network have previously been described for ASD using iPSC-derived cells<sup>12,24,27,28</sup>, which could be related to the cognitive impairment observed for the more compromised individuals<sup>29,30</sup>.

Our next point of analysis was focused on glutamate levels. Glutamate is the main excitatory neurotransmitter in the brain<sup>31,32</sup>. The glutamate/GABA-glutamine cycle is a metabolic pathway involving the release of glutamate from neurons, which is then taken up by astrocytes and converted into glutamine. Neurons subsequently take up glutamine to synthesize glutamate<sup>33</sup>. iPSC-derived neurons from CZS patients revealed a distinct pattern of glutamate production over time, but with a slight reduction in glutamate levels, when compared to the control group. Additionally, we compared the glutamate levels for the two CZS patients' groups since our mixed culture of neurons from CZS/B showed a lower proportion of astrocytes, which could interfere with the glutamate-glutamine cycle<sup>34,35</sup>. Despite that, glutamate levels were not significantly reduced between CZS/B and CZS/A groups. Alterations in glutamate levels have been previously reported in other *in vivo*<sup>36</sup> and *in vitro*<sup>37</sup> studies associated with reduced synapses. In addition, given that glutamate is a crucial neurotransmitter, diminished glutamate levels may contribute to neuronal dysfunction.

Considering the interplay between neurons and astrocytes, we also examined the functionality of astrocytes derived from CZS patients. Numerous studies have explored the involvement of astrocytes in CNS disorders, such as Alzheimer's<sup>38</sup> disease and ASD<sup>12</sup>. Astrocytes are neuroglial cells found in abundance in the CNS, being responsible for several functions, including neuronal support and nourishment, synaptogenesis<sup>39</sup> and maintenance of synapses, as well as neurotransmission clearance, among others<sup>40–46</sup>. Astrocytes derived from iPSC for CTRL and CZS patients exhibited characteristic morphology, which was similar between the two conditions, and GFAP expression. The glutamate-glutamine cycle was investigated again by analyzing the levels of glutamate in the astrocyte supernatant. The uptake of glutamate from the extracellular medium by astrocytes is a critical process that helps prevent neurotoxicity and may be altered by viral infections<sup>47</sup>. Although our work did not infect the astrocytes, our analysis revealed a significant reduction in glutamate concentration for the CZS group, when compared with the control group. This finding reinforces the neuronal impairment and brain dysfunction observed in the patient participants of this study.

Another parameter analyzed in our study was the intrinsic astrocyte cytokine production in the cell supernatant. Cytokines play important roles in inflammatory and protective immune responses against viral infections<sup>48</sup>. Moreover, an imbalance in cytokine production during early neurodevelopment can lead to long-term impacts, being reported as implicated in neurodevelopmental and neuropsychiatric disorders<sup>49–51</sup>. Cytokine increase can directly impact synaptogenesis<sup>12</sup>. Our findings revealed that CZS patients produced increased cytokine levels, when compared to the CTRL group.

Although further investigations related to genetics and epigenetics should be performed in embryonic-stage cells affected by the ZIKV during pregnancy in order to better understand the expression of the genes and respective product pathways affected by the ZIKV infection during pregnancy, studies using profiling genome-wide DNA methylation and iPSC-derived NPCs infected *in vitro* by the ZIKV showed significant changes in DNA methylation and gene expression. A study identified changes in DNA methylation profile in seven epigenetic modules of patients affected by the ZIKV infection during pregnancy<sup>52</sup>. In one of these modules, a known microcephaly gene (MCPH1) was differentially methylated<sup>52</sup>. This same study suggests that ZIKV may affect the methylation of a transcript, which is important to the stem cells of the developing embryo and plays an essential role in the CZS<sup>52</sup>. A study using *in vitro* ZIKV-infected iPSC-derived NPCs revealed that FOXP1 was downregulated after ZIKV infection<sup>53</sup>, a gene already described for ASD<sup>54</sup>, suggesting that this could be the first transcription factor related to neurodevelopment shifted due to viral infections.

During reprogramming, the genome of somatic cells undergoes rearrangements to re-establish the pluripotent stem cell pattern. Studies have shown that factor-based reprogramming can leave an epigenetic memory of the origin's tissue that may influence the desired differentiation<sup>55</sup>. Still, it has been shown iPSC derived from non-hematopoietic cells can retain residual methylation at loci required for hematopoietic fate, which manifests as reduced blood-forming potential *in vitro*<sup>55</sup>. Studies using somatic cell nuclear transfer (SCNT) showed that despite SCNT being able to generate functional totipotent cells that can give rise to entire organisms, such epigenetic modifications do not seem to be able to fully erase the donor cell-specific epigenetic patterns, resulting in the retention of epigenetic memory<sup>56</sup>. Moreover, iPSC generated through the expression of the four Yamanaka's factors<sup>57</sup> showed residual DNA methylation, histone modifications, and consequently preserving transcriptional and metabolic signatures from the donor cell<sup>58</sup>.



## Conclusion

This study successfully demonstrates the feasibility of CZS in vitro modeling, focusing on the characterization of cellular and molecular phenotypes. The observed impairment in the functioning of neurons and astrocytes in CZS patients is highly relevant and may contribute to reinforcing the clinical manifestations associated with this condition. However, further investigations are required to determine whether these characteristics are permanent, or a more targeted management is required to improve the phenotype of CZS-affected children during their growth.

## Material and methods

### Sample collection and culture of fibroblasts derived from skin biopsies

Samples were collected from a skin biopsy of CZS infants following the approval of the Ethics Committee (CAAE: 80,437,417.3.0000.5467). All skin biopsies from the infants were collected after signs of Informed Consent by a parent or legal guardian. CRTL samples were used from a biorepository obtained previously with approval by the Ethics Committee of the Institute of Biosciences CEP- ICB/USP (Protocol CEP/ICB-USP 1001, Biorepository: CAAE 58,219,416.0.0000.5467) and all experiments were performed according to the guidelines and regulations for human research.

Skin biopsies of infants were collected during surgeries already planned and recommended by physicians unrelated to this project. Samples were washed twice in PBS with a 5% antibiotic solution. Subsequently, the tissue was fragmented into smaller pieces and distributed evenly in a 6-well plate, gently pressing the fragments to facilitate tissue adhesion to the plate surface. Next, 2 mL of fibroblast culture medium was carefully added to the plate to avoid tissue detaching. The culture medium used consisted of DMEM-F12 (Life Technologies) supplemented with 15% of fetal bovine serum (FBS) (Life Technologies, CA, USA), 2% antibiotic-antifungal solution (100 U/mL penicillin, 100 µg/mL streptomycin, and 0.5 µg/mL amphotericin – Sigma, SL, USA Sigma-Aldrich), and 1% L-glutamine (Life Technologies). The culture was maintained at 37 °C in a 5% CO<sub>2</sub> atmosphere with controlled humidity.

### iPSC generation

Cellular reprogramming experiments were conducted using the episomal Epi5™ kit (Episomal iPSC Reprogramming Kit, Life Technologies, USA) and skin fibroblasts samples from patients and control subjects. The transfection of episomal plasmids was performed by electroporation using the Nucleofector™ system (Lonza, USA). The reprogramming factors Oct3/4, Sox-2, Klf4, and L-Myc, along with Lin28, mp53DD, and EBNA1, were included in the reprogramming kit.

After iPSC colonies formation, they were transferred to Matrigel-coated dishes (BD Biosciences, NJ, USA) to establish a feeder-free culture condition, keeping them in mTSeR-1 medium (Stem Cell Technologies, YVR, Canada), changing medium daily.

### Production of neuro progenitor cells (NPC)

The iPSC colonies medium was replaced with N2 medium (DMEM/F12 supplemented with 1 × N2—Life Technologies, CA, USA) containing two SMAD inhibitors: 1 µM dorsomorphin (Tocris, MO, USA) and 10 µM SB431542 (Stemgent, MA, USA). After 48 h, the colonies were gently scraped off the plate and transferred to suspension culture to form embryoid bodies (EB). The EB were cultured in N2 medium supplemented with dorsomorphin and SB431542 and maintained in suspension for 5 days (90 rpm).

Following the formation of EBs, they were collected and transferred to Matrigel-treated plates for adhesion. The cells were cultured in NBF medium (DMEM/F12 supplemented with 0.5 × N2, 0.5 × B27, 20 ng/mL bFGF-2, and 1% penicillin/streptomycin) to promote the formation of rosettes. The rosettes typically formed around 48 h and were maintained for up to 11 days. Daily monitoring was conducted to determine the appropriate time for collecting neural progenitor cells (NPC). The NPC were manually collected, dissociated, and plated onto polyornithine and laminin-coated plates. Expansion of the NPC was carried out using NBF culture medium.

### Production of neurons and astrocytes

For neuronal differentiation, NPC were plated in polyornithine and laminin-coated 24-well plates. On the day of plating, the cells were maintained in NBF medium. After 24 h, the medium was replaced with NB medium containing 10 µM ROCK pathway inhibitor (Y-27632, Calbiochem, Millipore, DA, Germany). The cells were cultured in this medium for 48 h, followed by a medium change to NB without FGF-2 and ROCK inhibitor. The NB medium was maintained for at least 28 days, with regular medium changes every 3–5 days to support neuronal differentiation.

To generate astrocytes, NPC were incubated with PBS at 37 °C for 5 min. The cells were then scraped using a cell scraper and transferred to six-well plates to form neurospheres in NBF medium with constant stirring at 90 rpm. The next day, FGF-2 was removed, and the ROCK pathway inhibitor was added at a final concentration of 5 µM. The cells were cultured in this medium for 48 h before switching to NB medium without FGF-2 for 1 week. On the 11th day of the protocol, AGM astrocyte growth medium (Astrocyte Growth Medium – Lonza, USA) was added and maintained for two weeks. Throughout these three weeks, the cells were constantly maintained under agitation at 90 rpm. At the end of the differentiation process, the neurospheres were plated on polyornithine and laminin-coated plates, allowing the release and growth of astrocytes along the entire plate surface.

### Immunofluorescence analyzes

For IF, cells were cultured in 24-well plates containing glass coverslips for cellular characterization until they reached approximately 80% of confluence. The cells were washed with PBS and fixed in 4% paraformaldehyde

(USB Corporation) for 15 min at room temperature. Fixed cells were washed with PBS and permeabilized using 0.1% Triton (Promega, WI, USA) for 15 min at room temperature. Subsequently, the cells were blocked with 2% Bovine Serum Albumin (BSA) solution in PBS for 4 h at room temperature and incubated overnight with the primary antibodies (in Supplementary Table 1A,B) at 4 °C. Following, the cells were washed with PBS and subjected to a second blocking step in 2% BSA solution for 1 h at room temperature, then incubated with secondary antibodies, such as Alexa Fluor 488, Alexa Fluor 555, and Alexa Fluor 647 (Life Technologies), for 1 h at room temperature. Cells were triple-washed with dPBS, and nuclei were stained using DAPI (Invitrogen, 1:10,000) diluted in a 1 × dPBS solution for 5 min. Cells were washed once after the DAPI addition with dPBS and mounted using Prolong Gold Antifade Reagent (Invitrogen). IPSC, NPC, and astrocyte immunoreactivity were evaluated using an EVOS fluorescence microscope (Thermo Fisher Scientific). Neuron images were captured using z-stacks on a DMI8 microscope (Leica Microsystems) using a 40 × magnification for morphology and a 63x/1.4NA magnification for puncta. Approximately 100 image stacks were acquired. The acquired images were submitted to deconvolution using the LAX-S software (Leica Microsystems) with the following parameters: *deconvolution set to "blind," number of iterations set to 10, and resize to 16-bit enabled*. The total number of astrocytes and neurons was evaluated by cell counting, considering the positive labeling for MAP-2 and GFAP.

### Quantification of synapses

An immunofluorescence protocol was conducted on neurons using specific antibodies to quantify the synapses. Neuronal filaments were labeled with anti-MAP2 antibodies, while presynaptic and postsynaptic proteins were labeled with anti-Synapsin 1 and anti-PSD-95 antibodies, respectively (Supplementary Table 1B).

For analysis, puncta counting was performed using ImageJ software. Colocalization of the presynaptic protein with the postsynaptic protein was used to identify and quantify synapses. The data obtained were then compared and statistically analyzed using GraphPad Prism 8 software (GraphPad) through analysis of variance (One way ANOVA) to assess any significant differences between experimental groups.

### Molecular analysis by quantitative PCR (qPCR)

Total cellular RNA was extracted from cells using the Trizol Reagent (Life Technologies) according to the manufacturer's instructions. Reverse transcriptase was performed using Super-Script III (Invitrogen) according to the manufacturer's instructions. Quantitative PCR (qPCR) analysis was carried out using SYBR green Supermix (Bio-Rad – CA, USA). Each sample was tested in triplicate to ensure accuracy and reproducibility. Oligonucleotides specific to the target genes were synthesized using sequences from the Harvard Primer Bank online (Supplementary Table 2). The qPCR cycle conditions were the following: initial polymerase activation and denaturation at 95 °C for 3 min, followed by 40 cycles of denaturation at 95 °C for 15 s, and annealing and extension at 60 °C for 1 min. GAPDH was used as the internal control (housekeeping gene) to normalize the gene expression data. All qPCR data were analyzed using absolute quantification. The data obtained were then compared and statistically analyzed using GraphPad Prism 8 software (GraphPad, CA, USA) through analysis of variance (Paired t-test and One way ANOVA) to determine any significant differences between groups.

### Glutamate analysis

The transport and uptake system of glutamate in neurons and astrocytes was assessed by measuring the efficiency of glutamate uptake from the culture medium using an ELISA assay following the manufacturer's instructions (Abnova kit (Abnova, Taipei City, Taiwan)). The assay normalization was based on nuclear staining quantification of DAPI using ImageJ.

The data obtained were analyzed using GraphPad Prism 8 software (GraphPad, CA, USA). Analysis of variance (Two-way ANOVA) was employed to compare and evaluate any significant differences in glutamate uptake among the experimental groups. This statistical analysis allowed for a comprehensive examination of the efficiency of glutamate transport and uptake in neurons and astrocytes, facilitating an understanding of their respective roles in glutamate homeostasis.

### Analysis of cytokines in astrocytes culture supernatant

Determination of the cytokines secreted by astrocytes was carried by Luminex xMAP technology with a 27-Plex panel magnetic beads kit for quantification of the following analytes: IL-1 $\beta$ , IL-1 $\alpha$ , IL-2, IL-4, IL-5, IL-6, IL-7, IL-8, IL-9, IL-10, IL-12 (p70), IL-13, IL-15, IL-17, eotaxin, bFGF, GCSE, GM-CSF, IFN- $\gamma$ , CXCL-10 (IP-10), MCP-1 (MCAF), MIP-1 $\alpha$ , MIP-1 $\beta$ , PDGF-BB, CCL5 (RANTES), TNF- $\alpha$  and VEGF. The assay development was carried out following the manufacturer recommendations.

Statistical analysis was performed using GraphPad Prism 8 software (GraphPad, CA, USA) to evaluate the data. Analysis of variance (One way ANOVA) was employed to compare and assess any significant differences between the experimental groups. This statistical analysis allowed for a comprehensive understanding of the cytokine profiles and their variations among the samples.

### Ethics approval and consent to participate

Ethical approval for the study was granted by the Ethical Committee from the Institute of Biomedical Sciences from the University of São Paulo, Brazil (CAAE: 80437417.3.0000.5467).

### Data availability

The datasets generated and analyzed during the current study are not publicly available due restriction by the Ethic Committee but are available from the corresponding author on reasonable request.

Received: 1 December 2023; Accepted: 18 June 2024

Published online: 03 August 2024

# References

1. Pielnaa, P. *et al.* Zika virus-spread, epidemiology, genome, transmission cycle, clinical manifestation, associated challenges, vaccine and antiviral drug development. *Virology* **543**, 34–42. <https://doi.org/10.1016/j.virol.2020.01.015> (2020).
2. Vianna, P. *et al.* Zika Virus as a possible risk factor for autism spectrum disorder. *Neuroimmunomodulation* **25**(5–6), 320–327 (2018).
3. Lum, F. M. *et al.* Zika virus infects human fetal brain microglia and induces inflammation. *Clin. Infect. Dis. Off. Publ. Infect. Dis. Soc. Am.* **64**(7), 914–920 (2017).
4. Massrali, A., Adhya, D., Srivastava, D. P., Baron-Cohen, S. & Kotter, M. R. Virus-induced maternal immune activation as an environmental factor in the etiology of autism and schizophrenia. *Front. Neurosci.* **16**, 943903 (2022).
5. Mahmoud, S., Gharagozloo, M., Simard, C. & Gris, D. Astrocytes maintain glutamate homeostasis in the CNS by controlling the balance between glutamate uptake and release. *Cells* **8**(2), 184 (2019).
6. Santi, L. *et al.* Zika virus infection associated with autism spectrum disorder: A case report. *Neuroimmunomodulation* **28**(4), 229–232 (2021).
7. Lauritsen, M. B. Autism spectrum disorders. *Eur. Child Adolesc. Psychiatry* **22**, S37–S42 (2013).
8. Ashwood, P. *et al.* Decreased transforming growth factor beta1 in autism: A potential link between immune dysregulation and impairment in clinical behavioral outcomes. *J. Neuroimmunol.* **204**, 149–153 (2008).
9. Li, X. *et al.* Elevated immune response in the brain of autistic patients. *J. Neuroimmunol.* **207**, 111–116 (2009).
10. Wei, H. *et al.* IL-6 is increased in the cerebellum of autistic brain and alters neural cell adhesion, migration and synaptic formation. *J. Neuroinflamm.* **8**, 52 (2011).
11. Vargas, D. L., Nascimbene, C., Krishnan, C., Zimmerman, A. W. & Pardo, C. A. Neuroglial activation and neuroinflammation in the brain of patients with autism. *Ann. Neurol.* **57**, 67–81 (2005).
12. Russo, F. B. *et al.* Modeling the interplay between neurons and astrocytes in autism using human induced pluripotent stem cells. *Biol. Psychiatry* **83**(7), 569–578 (2018).
13. Okano, H. & Morimoto, S. iPSC-based disease modeling and drug discovery in cardinal neurodegenerative disorders. *Cell Stem Cell* **29**(2), 189–208 (2022).
14. Qian, L. & Tcw, J. Human iPSC-based modeling of central nerve system disorders for drug discovery. *Int. J. Mol. Sci.* **22**(3), 1203 (2021).
15. Aboul-Soud, M. A. M., Alzahrani, A. J. & Mahmoud, A. Induced pluripotent stem cells (iPSCs)-roles in regenerative therapies, disease modelling and drug screening. *Cells* **10**(9), 2319 (2021).
16. Rouhani, F. *et al.* Genetic background drives transcriptional variation in human induced pluripotent stem cells. *PLoS Genet.* **10**(6), e1004432 (2014).
17. Marchetto, M. C. N. *et al.* Transcriptional signature and memory retention of human-induced pluripotent stem cells. *PLoS ONE* **4**(9), e7076 (2009).
18. Caires-Junior, L. C. *et al.* Discordant congenital Zika syndrome twins show differential in vitro viral susceptibility of neural progenitor cells. *Nat. Commun.* **9**, 475. <https://doi.org/10.1038/s41467-017-02790-9> (2018).
19. D’aiuto, L. *et al.* Large-scale generation of human iPSC-derived neural stem cells/early neural progenitor cells and their neuronal differentiation. *Organogenesis* **10**(4), 365–377 (2014).
20. Cugola, F. R. *et al.* The Brazilian Zika virus strain causes birth defects in experimental models. *Nature* **534**(7606), 267–271 (2016).
21. Caires-Júnior, L. C. *et al.* Discordant congenital Zika syndrome twins show differential in vitro viral susceptibility of neural progenitor cells. *Nat. Commun.* **9**(1), 475 (2018).
22. Qian, X. *et al.* Brain-region-specific organoids using mini-bioreactors for modeling ZIKV exposure. *Cell* **165**(5), 1238–1254 (2016).
23. Marchetto, M. C. *et al.* A model for neural development and treatment of Rett syndrome using human induced pluripotent stem cells. *Cell* **143**(4), 527–539 (2010).
24. Marchetto, M. C. *et al.* Altered proliferation and networks in neural cells derived from idiopathic autistic individuals. *Mol. Psychiatry* **22**(6), 820–835 (2017).
25. Rosa-Fernandes, L. *et al.* Zika virus impairs neurogenesis and synaptogenesis pathways in human neural stem cells and neurons. *Front. Cell. Neurosci.* **13**, 64 (2019).
26. Figueiredo, C. P. *et al.* Zika virus replicates in adult human brain tissue and impairs synapses and memory in mice. *Nat. Commun.* **10**(1), 3890 (2019).
27. Beltrão-Braga, P. C. B. & Muotri, A. R. Modeling autism spectrum disorders with human neurons. *Brain Res.* **1656**, 49–54 (2017).
28. Williams, E. C. *et al.* Mutant astrocytes differentiated from Rett syndrome patients-specific iPSC have adverse effects on wildtype neurons. *Human Mol. Genet.* **23**, 2968–2980 (2014).
29. Maezawa, I. & Jin, L. W. Rett syndrome microglia damage dendrites and synapses by the elevated release of glutamate. *J. Neurosci.* **30**, 5346 (2010).
30. Spooren, W., Lindemann, L., Ghosh, A. & Santarelli, L. Synapse dysfunction in autism: A molecular medicine approach to drug discovery in neurodevelopmental disorders. *Trends Pharmacol. Sci.* **33**, 669–684 (2012).
31. Hao, Y. & Plested, A. J. R. Seeing glutamate at central synapses. *J. Neurosci. Methods* **375**, 109531 (2022).
32. Meldrum, B. S. Glutamate as a neurotransmitter in the brain: review of physiology and pathology. *J. Nutr.* **130**, 1007–1015 (2000).
33. Hackett, J. T. & Ueda, T. Glutamate release. *Neurochem. Res.* **40**(12), 2443–2460 (2015).
34. Araque, A., Parpura, V., Sanzgiri, R. P. & Haydon, P. G. Glutamate-dependent astrocyte modulation of synaptic transmission between cultured hippocampal neurons. *Eur. J. Neurosci.* **10**(6), 2129–2142 (1998).
35. Haydon, P. G. & Carmignoto, G. Astrocyte control of synaptic transmission and neurovascular coupling. *Physiol. Rev.* **86**(3), 1009–1031 (2006).
36. Potier, B. *et al.* Reduction in glutamate uptake is associated with extrasynaptic NMDA and metabotropic glutamate receptor activation at the hippocampal CA1 synapse of aged rats. *Aging Cell* **9**(5), 722–735 (2010).
37. Talantova, M. *et al.* Aβ induces astrocytic glutamate release, extrasynaptic NMDA receptor activation, and synaptic loss. *Proc. Natl. Acad. Sci. U. S. A.* **110**(27), E2518–E2527 (2013).
38. Simpson, J. E. *et al.* Astrocyte phenotype in relation to Alzheimer-type pathology in the ageing brain. *Neurobiol. Aging* **31**, 578–590 (2010).
39. Phatmani, H. & Maniatis, T. Astrocytes in neurodegenerative disease. *Cold Spring Harbor Perspect. Biol.* **7**(6), a020628 (2015).
40. Ullian, E. M., Christopherson, K. S. & Barres, B. A. Role for glia in synaptogenesis. *Glia* **47**, 209 (2004).
41. Christopherson, K. S. *et al.* Thrombospondins are astrocyte-secreted proteins that promote CNS synaptogenesis. *Cell* **120**, 421–433 (2005).
42. Johnson, M. A., Weick, J. P., Pearce, R. A. & Zhang, S. C. Functional neural development from human embryonic stem cells: Accelerated synaptic activity via astrocyte coculture. *J. Neurosci.* **27**(12), 3069–3077 (2007).
43. Eroglu, C. & Barres, B. A. Regulation of synaptic connectivity by glia. *Nature* **468**(7321), 223–231 (2010).



44. Zhang, Y. & Barres, B. A. Astrocyte heterogeneity: An underappreciated topic in neurobiology. *Curr. Opin. Neurobiol.* **20**(5), 588–594 (2010).
45. Colangelo, A. M., Alberghina, L. & Papa, M. Astroglisis as a therapeutic target for neurodegenerative diseases. *Neurosci. Lett.* **565**, 59–64 (2014).
46. Pekny, M., Wilhelmsson, U. & Pekna, M. The dual role of astrocyte activation and reactive gliosis. *Neurosci. Lett.* **565**, 30–38 (2014).
47. Verkhratsky, A. & Nedergaard, M. Physiology of astroglia. *Physiol. Rev.* **98**(1), 239–389 (2018).
48. Koyama, S., Ishii, K. J., Coban, C. & Akira, S. Innate immune response to viral infection. *Cytokine* **43**(3), 336–341 (2008).
49. Rahman, M. M. Exploring the management approaches of cytokines including viral infection and neuroinflammation for neurological disorders. *Cytokine* **157**, 155962 (2022).
50. Elgueta, D. *et al.* Consequences of viral infection and cytokine production during pregnancy on brain development in offspring. *Front. Immunol.* **13**, 816619 (2022).
51. Jiang, N. M., Cowan, M., Moonah, S. N. & Petri, W. A. The impact of systemic inflammation on neurodevelopment. *Trends Mol. Med.* **24**(9), 794–804. <https://doi.org/10.1016/j.molmed.2018.06.008> (2018).
52. Anderson, D. *et al.* Zika virus changes methylation of genes involved in immune response and neural development in Brazilian babies born with congenital microcephaly. *J. Infect. Dis.* **223**(3), 435–440 (2021).
53. Lottini, G. *et al.* Zika virus induces FOXG1 nuclear displacement and downregulation in human neural progenitors. *Stem Cell Rep.* **17**(7), 1683–1698 (2022).
54. Mariani, J. *et al.* FOXG1-dependent dysregulation of GABA/glutamate neuron differentiation in autism spectrum disorders. *Cell* **162**(2), 375–390 (2015).
55. Kim, K. *et al.* Epigenetic memory in induced pluripotent stem cells. *Nature* **467**(7313), 285–290 (2010).
56. Firas, J. *et al.* Epigenetic memory in somatic cell nuclear transfer and induced pluripotency: Evidence and implications. *Differentiation* **88**(1), 29–32 (2014).
57. Takahashi, K. & Yamanaka, S. Induction of pluripotent stem cells from mouse embryonic and adult fibroblast cultures by defined factors. *Cell* **126**(4), 663–676 (2006).
58. Polo, J. M. *et al.* Cell type of origin influences the molecular and functional properties of mouse induced pluripotent stem cells. *Nat. Biotechnol.* **28**(8), 848–855 (2010).

## Acknowledgements

We thank the NGO "The Tooth Fairy Project" and all individuals and their families who donated biological samples.

## Author contributions

C.B. and P.C.B.B.B. conceptualized the study. CB and FHL reprogrammed the fibroblast from CZS children. C.B., F.P., and F.B.R. produced the CNS cells. C.B., F.B.R., and A.C.M. analyzed the IF. P.E.C.L. performed the cytokine analysis by Luminex. C.B., F.B.R., and P.C.B.B.B. performed and analyzed all the statistical analyses. V.V.d.L. and P.J. collected the patient samples. V.V.d.L. conducted the cohort study. C.B., V.V.d.L., M.C.S., A.B.C., F.B.R., and P.C.B.B.B. analyzed and discussed the data and wrote the manuscript. All authors read and agreed with the manuscript publication.

## Funding

This work was supported by grants from the State of São Paulo Research Foundation-FAPESP (Thematic project No. 2016/02978-6 to MCS, and regular grant 2018/16748-8 to PCBBB), the NGO "The Tooth Fairy Project", CNPq and FAPESP for PhD fellowships (#149909/2016-0, #169784/2017-7, #2011/20683-0 and 2013/08844-3). PCBBB and MCS were recipients of the Brazilian National Research and Technology Council (CNPq), Research Award #304663/2021-2 and #311855/2015-6, respectively. FHL was supported by DTI Post-doctoral fellowship (#384519/2010-5). The Leica-Dmi8 microscope used in this study was obtained with funding from FAPESP (2015/02654-3).

## Competing interests

The authors declare no competing interests.

## Additional information

**Supplementary Information** The online version contains supplementary material available at <https://doi.org/10.1038/s41598-024-65392-8>.

**Correspondence** and requests for materials should be addressed to F.B.R. or P.B.-B.

**Reprints and permissions information** is available at [www.nature.com/reprints](http://www.nature.com/reprints).

**Publisher's note** Springer Nature remains neutral with regard to jurisdictional claims in published maps and institutional affiliations.

**Open Access** This article is licensed under a Creative Commons Attribution-NonCommercial-NoDerivatives 4.0 International License, which permits any non-commercial use, sharing, distribution and reproduction in any medium or format, as long as you give appropriate credit to the original author(s) and the source, provide a link to the Creative Commons licence, and indicate if you modified the licensed material. You do not have permission under this licence to share adapted material derived from this article or parts of it. The images or other third party material in this article are included in the article's Creative Commons licence, unless indicated otherwise in a credit line to the material. If material is not included in the article's Creative Commons licence and your intended use is not permitted by statutory regulation or exceeds the permitted use, you will need to obtain permission directly from the copyright holder. To view a copy of this licence, visit <http://creativecommons.org/licenses/by-nc-nd/4.0/>.

© The Author(s) 2024